World Academy of Science, Engineering and Technology
International Journal of Chemical and Molecular Engineering
Vol:10, No:11, 2016

Microkinetic Modelling of NO Reduction on Pt Catalysts

Vishnu S. Prasad, Preeti Aghalayam

***Abstract*—**The major harmful automobile exhausts are nitric oxide (NO) and unburned hydrocarbon (HC). Reduction of NO using unburned fuel HC as a reductant is the technique used in hydrocarbon-selective catalytic reduction (HC-SCR). In this work, we study the microkinetic modelling of NO reduction using propene as a reductant on Pt catalysts. The selectivity of NO reduction to N_2O is detected in some ranges of operating conditions, whereas the effect of inlet O_2% causes a number of changes in the feasible regimes of operation.

***Keywords*—**Microkinetic modelling, NOx, Pt on alumina catalysts, selective catalytic reduction.

I. Introduction

AUTOMOBILE exhausts have a major contribution to air pollution. The important air pollutants from automobile exhausts are oxides of carbon, nitrogen and unburnt HCs, which have an adverse effect on environment and human health. HC-SCR is one of the potential methods to reduce NO_x as well as unburned HC emissions.

Various reductants such as propene, propane, octane, and methane [1] and catalysts such as Platinum group metals, Ag, Au and zeolites [1], [2] are proposed for HC-SCR. Pt catalysts have been reported to have a good low temperature activity and water tolerance as compared to zeolite catalysts [3]. Comparisons of performance using different PGM catalysts is shown in literature [1]. It has been reported that Ag catalysts yield high conversions for NO and HC, silver loading and effect of preparation methods are also extensively studied in the literature [4], [5].

In this work, a detailed modelling study is undertaken in order to identify and analyze various regimes for HC-SCR that occur as the inlet O_2 concentration is varied. A microkinetic model involving several gas-phase and surface-adsorbed species is presented and rate parameters are estimated from theoretical calculations. The reaction mechanism is incorporated in ideal reactor modules and various features including the conversions of NO and HC, and the selectivity to N_2 and N_2O are examined as a function of inlet concentrations and reactor temperature.

II. Methodology

The modelling and simulations are performed using the commercial CHEMKIN software package. A detailed surface reaction mechanism is incorporated in an isothermal Perfectly Stirred Reactor model. The inlet concentrations for HC (C_3H_6) and NO are 2000 ppm and 1000 ppm, concentration of O_2 is varied from 0% to 3% and the carrier gas is taken as Argon. A reactor volume of 2 cm^3 is considered in the simulations. The inlet volumetric flow rate is 50 cm^3/s, the pressure inside the reactor is taken as 1 bar. The catalyst surface area is taken as 180 m^2/g [6] and the residence time is 0.04 s. The reactor temperature is varied from 200 ^{0}C to 650 ^{0}C.

III. Surface Reaction Mechanism

A detailed surface reaction from the literature [7], consisting of 52 reactions, is first taken in this study. The following modifications are made to this reaction schema:

- Surface coverage dependence of activation energies are eliminated, and all activation energies are taken as constants. As the coverage dependence was fitted to experiments in the literature [7], we expect that our modified reaction mechanism is more general.
- The N_2O surface mechanism (4 reactions) was developed earlier in our group [8] and is appended to the literature reaction mechanism. One of the goals of this work is to analyze selectivities, and this is an important component that is missing in earlier work.

The final surface reaction mechanism consists of 56 reactions with 9 gaseous species and 19 surface species & is shown in Table I. The activation energy and pre-exponential values for the reactions are taken from literature, the adsorption, desorption and surface reactions for N_2O reactions are developed in our group [8]. The mechanism consists of 9 adsorption reactions, 10 desorption reactions and 37 surface reactions in the surface reaction mechanism. The 9 gas species considered in the mechanism are O_2, C_3H_6, H_2, H_2O, CO_2, CO, NO, N_2O and N_2. The 19 surface species considered are Pt(S), O(S), C_3H_6(S), C_3H_5(S), OH(S), H(S), H_2O(S), CO_2(S), CO(S), C(S), CC_2H_5(S), C_2H_3(S), CH_2(S), CH_3(S), CH(S), CH_3CO(S), NO(S), N_2O(S) and N(S).

IV. Reactor Scale Model

The steady state simulations are obtained using an isothermal perfectly stirred reactor. The equations used are mass balance for surface species, gas species and site conservation.

Surface intermediates mass balance

$$\frac{\Gamma}{N_A}\frac{d\theta_k}{dt} = \sum_{j=1}^{nrxns} \nu_{kj} R_j \qquad \text{(k=1, 2, ...n surface)} \qquad (1)$$

Vishnu S Prasad, is with the Indian Institute of Technology, Chennai, 600036 India (e-mail: vshnprasad0@gmail.com).

Preeti Aghalayam, is with the Indian Institute of Technology, Chennai, 600036 India (phone: +91 44 2257 4153; e-mail: preeti@iitm.ac.in).

TABLE I
DETAILED SURFACE REACTION MECHANISM OF NO REDUCTION USING PROPENE

NO.	Reactions	Pre-exponential factor k_0 (s^{-1})/sticking coefficient	Activation energy E_a (kj/mol)
ADSORPTION		**Pt**	**Pt**
1	$O_2 + 2* \rightarrow 2O^*$	0.007	0
2	$C_3H_6 + 2^* \rightarrow C_3H_6{}^*$	0.98	0
3	$C_3H_6 + O^* + * \rightarrow C_3H_5{}^* + OH^*$	0.005	0
4	$H_2 + 2* \rightarrow 2H^*$	0.046	0
5	$H_2O + * \rightarrow H_2O^*$	0.75	0
6	$CO_2 + * \rightarrow CO_2{}^*$	0.005	0
7	$CO + * \rightarrow CO^*$	0.84	0
8	$NO + * \rightarrow NO^*$	0.85	0
9	$N_2O + * \rightarrow N_2O^*$	0.001	0
		DESORPTION	
10	$2O^* \rightarrow O_2 + 2*$	7.54×10^{12}	232.2
11	$C_3H_6{}^* \rightarrow C_3H_6 + 2^*$	1.0×10^{13}	72.7
12	$C_3H_5{}^* + OH^* \rightarrow C_3H_6 + O^* + *$	7.54×10^{12}	31
13	$2H^* \rightarrow H_2 + 2*$	7.54×10^{12}	67.4
14	$H_2O^* \rightarrow * + H_2O$	1.0×10^{13}	40.3
15	$CO_2{}^* \rightarrow CO_2 + *$	1.0×10^{13}	27.1
16	$CO^* \rightarrow CO + *$	1.0×10^{13}	136.4
17	$NO^* \rightarrow NO + *$	1.0×10^{16}	140
18	$N_2O^* \rightarrow N_2O + *$	1.0×10^{13}	23.4
19	$N^* + N^* \rightarrow N_2 + 2*$	7.54×10^{12}	113.9
		SURFACE REACTION	
20	$C_3H_5{}^* + 5O^* + 2* \rightarrow 5OH^* + 3C^*$	7.54×10^{12}	95
21	$C_3H_6{}^* \rightarrow H^* + CC_2H_5{}^*$	1.0×10^{13}	75.4
22	$CC_2H_5{}^* + H^* \rightarrow C_3H_6{}^*$	7.54×10^{12}	48.8
23	$CC_2H_5{}^* + * \rightarrow C_2H_3{}^* + CH_2{}^*$	7.54×10^{12}	108.2
24	$C_2H_3{}^* + CH_2{}^* \rightarrow CC_2H_5{}^* + *$	7.54×10^{12}	3.2
25	$C_2H_3{}^* + * \rightarrow CH_3{}^* + C^*$	7.54×10^{12}	46
26	$CH_3{}^* + C^* \rightarrow C_2H_3{}^* + *$	7.54×10^{12}	46.9
27	$CH_3{}^* + * \rightarrow CH_2{}^* + H^*$	2.57×10^{13}	70.4
28	$CH_2{}^* + H^* \rightarrow CH_3{}^* + *$	6.30×10^{13}	0
29	$CH_2{}^* + * \rightarrow CH^* + H^*$	1.42×10^{14}	59.2
30	$CH^* + H^* \rightarrow CH_2{}^* + *$	6.30×10^{13}	0
31	$CH^* + * \rightarrow C^* + H^*$	6.30×10^{13}	0
32	$C^* + H^* \rightarrow CH^* + *$	2.55×10^{13}	138
33	$C_2H_3{}^* + O^* \rightarrow * + CH_3CO^*$	7.54×10^{10}	62.3
34	$CH_3CO^* + * \rightarrow C_2H_3{}^* + O^*$	7.54×10^{12}	196.7
35	$CH_3{}^* + CO^* \rightarrow * + CH_3CO^*$	7.54×10^{12}	82.9
36	$CH_3CO^* + * \rightarrow CH_3{}^* + CO^*$	7.54×10^{12}	0
37	$CH_3{}^* + O^* \rightarrow CH_2{}^* + OH^*$	7.54×10^{12}	36.6
38	$CH_2{}^* + OH^* \rightarrow CH_3{}^* + O^*$	7.54×10^{12}	25.1

NO.	Reactions	Pre-exponential factor k_0 (s^{-1})/sticking coefficient	Activation energy E_a (kj/mol)
39	$CH_2^* + O^* \rightarrow CH^* + OH^*$	$7.54x10^{12}$	25.1
40	$CH^* + OH^* \rightarrow CH_2^* + O^*$	$7.54x10^{12}$	25.2
41	$CH^* + O^* \rightarrow C^* + OH^*$	$7.54x10^{12}$	25.1
42	$C^* + OH^* \rightarrow CH^* + O^*$	$7.54x10^{12}$	224.8
43	$O^* + H^* \rightarrow OH^* + *$	$7.54x10^{12}$	11.5
44	$OH^* + * \rightarrow O^* + H^*$	$1.17x10^{14}$	74.9
45	$OH^* + H^* \rightarrow H_2O^* + *$	$7.54x10^{12}$	17.4
46	$H_2O^* + * \rightarrow OH^* + H^*$	$7.46x10^{12}$	73.6
47	$OH^* + OH^* \rightarrow H_2O^* + O^*$	$7.54x10^{12}$	48.2
48	$H_2O^* + O^* \rightarrow OH^* + OH^*$	$4.794x10^{11}$	41
49	$CO^* + O^* \rightarrow CO_2^* + *$	$7.54x10^{11}$	108
50	$CO_2^* + * \rightarrow CO^* + O^*$	$7.54x10^{12}$	165.1
51	$C^* + O^* \rightarrow CO^* + *$	$7.54x10^{12}$	0
52	$CO^* + * \rightarrow C^* + O^*$	$7.54x10^{12}$	218.5
53	$NO^* + * \rightarrow N^* + O^*$	$1.02x10^{12}$	107.8
54	$N^* + O^* \rightarrow NO^* + ^*$	$7.54x10^{12}$	128.1
55	$NO^* + N^* \rightarrow N_2O^* + ^*$	$1.0x10^{12}$	87.8
56	$N_2O^* + ^* \rightarrow NO^* + N^*$	$1.0x10^{12}$	15.1

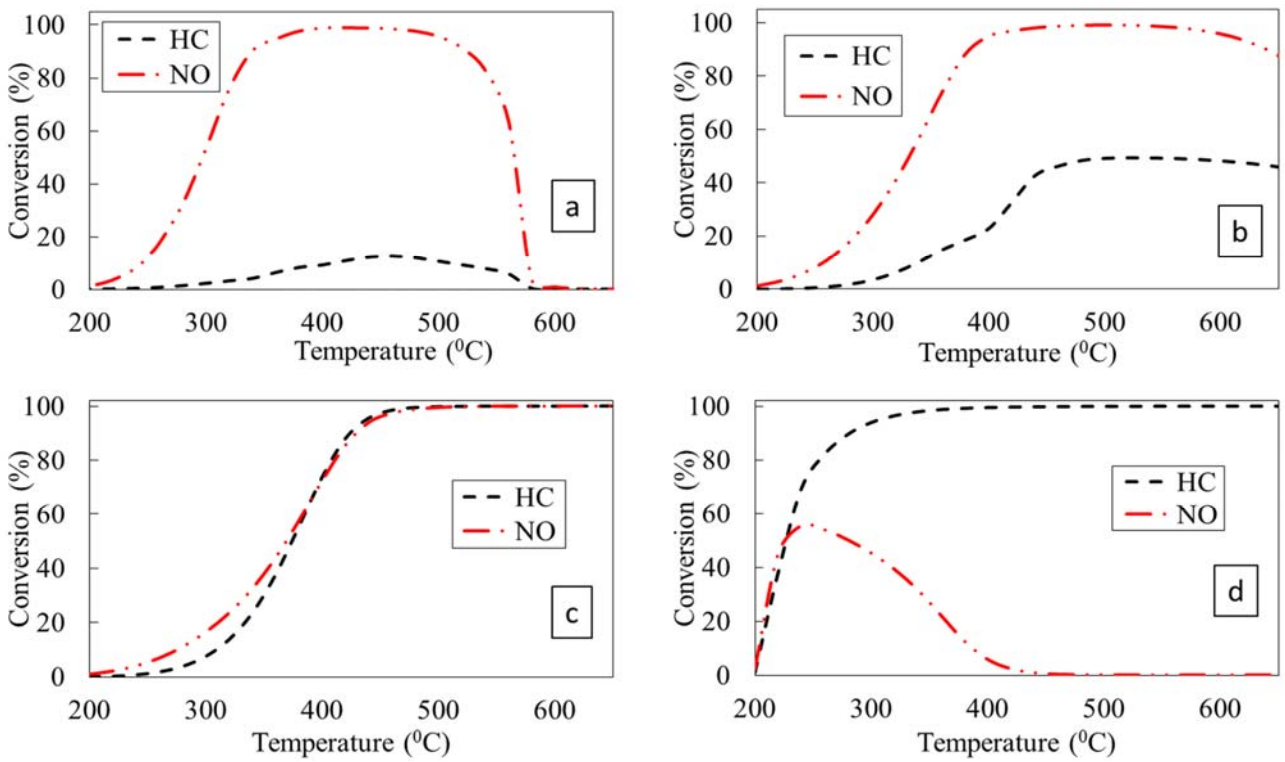

Fig. 1 (a) NO and HC conversion at 0% inlet O_2 vs reactor temperature (b) NO and HC conversion at 0.1% inlet O_2 vs reactor temperature (c) NO and HC conversion at 0.6% inlet O_2 vs reactor temperature (d) NO and HC conversion at 3% inlet O_2 vs reactor temperature

Mass balance for gas-phase species

$$\frac{dC_i}{dt} = \frac{(C_i^0 - C_i)}{\tau} + a_v * (\sum_{j=1}^{nrxns} \nu_{ij} R_j) \text{ (i=1, 2,...n gas)} \quad (2)$$

Site conservation

$$\theta_* = 1 - \sum_{k=1}^{nsurface} \theta_k \quad (3)$$

There are 19 surface intermediate mass balance equations, 9 gas phase species equations and 1 site conservation equations. Here, Γ is the site density of the catalyst, N_A is the Avogadro number, θ_k is the surface coverage of the kth species, C_i^0 is the inlet concentration of the i th species, C_i is the outlet concentration of the i th species, a_v is the surface area/volume ratio of the catalyst, and τ is the space time.

V. Results and Discussion

The inlet gas concentrations of NO and C_3H_6 (which represent HC) are 1000 ppm and 2000 ppm. The O_2 concentrations are varied from 0% to 3%. Various regimes are obtained due to change in the O_2 concentrations and N_2 selectivity as the reactor temperature and O_2 concentration variation is also studied.

At 0% O_2 (Fig. 1 (a)) the NO conversion increases from 0% at 200 ^{0}C to 100% at 400 ^{0}C and the conversion stays at 100% till 480 ^{0}C. After 480 ^{0}C the NO conversion decreases steeply and reaches 0% at 580 ^{0}C. The same trend is seen for HC conversion as well (Fig. 1 (a)), here conversion starts at 260 ^{0}C and reaches the maximum conversion of 12% at 460 ^{0}C and decreases at higher temperatures. When reactor temperatures are higher than 580 ^{0}C the conversions of both NO and HC are 0%.

As the O_2 increases to 0.1% (Fig. 1 (b)), the NO conversion starts at 200 ^{0}C and reaches 100% conversion at 440 ^{0}C, at high temperatures i.e. after 560 ^{0}C the NO conversion decreases slightly. Similarly, the HC conversion (Fig. 1 (b)) reaches a maximum of 50% at 520 ^{0}C and decreases slightly after 560 ^{0}C.

When the inlet O_2 % is increased to 0.6% (Fig. 1 (c)) the NO conversion increases from 0% to 100 % conversion at 460 ^{0}C, there is no decrease in the conversions at higher temperatures. The HC conversion (Fig. 1 (c)) follows the same trend, the conversions reaches 100% at 460 ^{0}C and up to 650 ^{0}C there is no decrease in conversions.

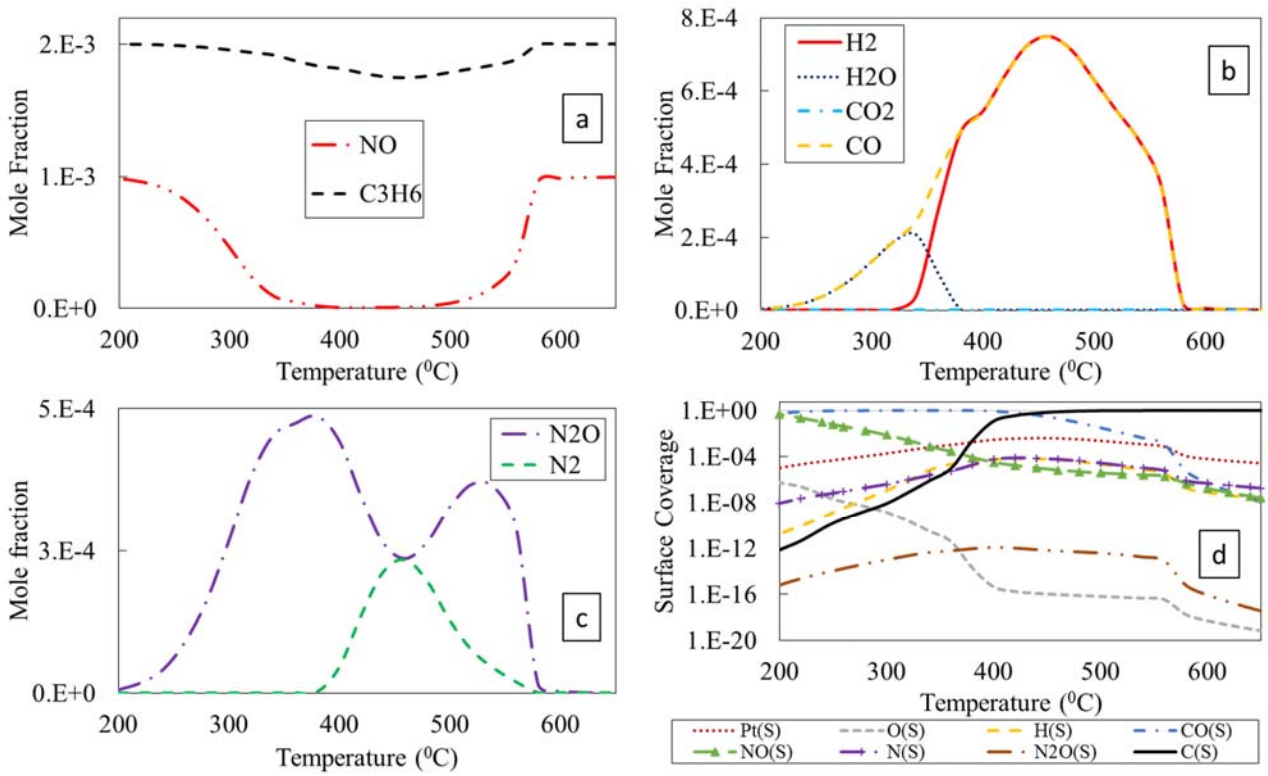

Fig. 2 (a) Mole fraction of reactants at 0% inlet O_2 vs reactor temperature (b) Mole fraction of H_2, H_2O, CO_2 and CO at 0% inlet O_2 vs reactor temperature (c) Mole fraction of N_2O and NO at 0% inlet O_2 vs reactor temperature (d) Surface coverage at 0% inlet O_2 vs reactor temperature

As the inlet O_2 % is increased to 3% (Fig. 1 (d)), the NO conversions increases to a maximum of 55% at 240 ^{0}C and decreases as the temperature increases. At 440 ^{0}C, the NO conversion reaches 0%, there is no NO conversion beyond 440 ^{0}C. The HC conversion (Fig. 1 (d)) increases steeply and reaches 100% conversion at 360 ^{0}C and remains high at higher temperatures as well. Thus, the behaviour of the HC-SCR reactor as the inlet O2 is increased from 0-3% demonstrates several distinct changes.

A. NO and HC Regimes for Pt Catalyst

Based on the conversions of NO and HC for different O_2 %, four different operating regimes are identified [9]:

a) Coking 1
b) Coking 2
c) Optimal operating regime
d) Oxygen poisoned regime

Coking 1 regime: This regime is seen at 0% O_2 in the feed (Fig. 1 (a)) where the conversions decrease to 0% at higher

temperatures, greater than 580 ^{0}C. In this regime, C(S) species cover the catalyst completely and irreversibly, and does not allow for any other species to adsorb. This kills the reactivity at higher temperatures and renders the catalyst inactive for all reactions. [9].

Coking 2 Regime: This regime is seen at very low oxygen percentage in the feed (0.1-0.2% O_2), In this regime only at very high temperatures, greater than 620 ^{0}C the coking phenomena is observed (Fig. 1 (b)). In this regime, the poisoning of the catalyst by coke formed from the HC is somewhat mitigated due to the presence of small amount of O2 in the inlet [9].

Optimal operating regime: This regime is seen at an oxygen percentage (0.5-0.7% O_2). In this regime, the conversions of NO and HC are very high, this should be the optimal operating condition of the feed O_2 for the maximum conversions of NO & HC [9]. A perfect balance is maintained here, and the catalyst is very effective at these conditions.

Oxygen poisoned regime: This regime is seen at high oxygen percentage (>3%). In this regime the conversions of NO are low but the conversions of HC are very high, Here, the catalyst is "poisoned" by the O(S) species so instead of the reductive environment of the catalyst, an oxidative environment results. Compared to the coking regime, here, the oxidation of HC can occur though the reduction of NO cannot [9].

B. Analysis of Species in the Various Regimes

The mole fractions and the surface coverages of the gas and surface species are analysed as the percentage of O_2 increases, four cases have been considered here 0% O_2, 0.1% O_2, 0.6% O_2, 3% O_2.

At 0% O_2 (Fig. 2 (d)), as the temperature increases from 200 ^{0}C, the catalyst is mainly covered by CO(S) species till 440 ^{0}C. At temperatures greater than 440 ^{0}C, the C(S) is the predominant species, while at temperature greater than 560 ^{0}C, C(S) species cover the catalyst completely. As the temperature increases from 200 ^{0}C, the catalyst is reductive in nature so there is a high conversion of NO, seen in Fig. 2 (a). The decrease in the conversions after 560 ^{0}C is due to poisoning of the catalyst by coke C(S). The HC conversions are low due to the absence of O_2 in the feed.

The main gaseous products are N_2, N_2O, CO, H_2O and H_2 (Figs. 2 (b), (c)). The CO_2 formation is very low due to the absence of O_2 in the feed. The N_2 formation is in the range of 380-550 ^{0}C with the maximum formation at 440 ^{0}C, even though there is high conversion of NO at 0% O_2 the NO conversion is mainly to N_2O at low temperatures 250 ^{0}C to 400 ^{0}C as well as at high temperatures 500 ^{0}C to 580 ^{0}C. The selectivity of N_2 is limited to a narrow range of temperature from 420 ^{0}C to 500 ^{0}C. Overall, this regime is not attractive from viewpoint of selectivity.

At 0.1% O_2, the reactants O_2 and NO conversion are 100% (Fig. 3 (a)) at temperatures above 400 ^{0}C, HC reaches a maximum conversion of 49% at 460 ^{0}C, as the temperature increases the conversion of all the reactants increase till 600 ^{0}C after 600 ^{0}C the surface coverage of C(S) species increases (Fig. 3 (d)) and leads to catalyst deactivation. In this region at low temperatures, the surface is covered by CO(S) species and a reductive environment is provided, as the temperature increases the C(S) species increases and covers the catalyst surface completely.

The main gaseous products are H_2, H_2O, CO, N_2 and N_2O. The CO_2 formation is very less at inlet O_2 concentration of 0.1% (Figs. 3 (b), (c)). At low temperatures, the main gaseous products are H_2O and N_2O. As the temperature increases from 400 ^{0}C, the main products are H_2, H_2O and N_2. At high temperatures greater than 620 ^{0}C the mole fraction of the gaseous products decreases due to coking. This regime is similar to the earlier case, and is unattractive from view point of conversions/selectivity at higher temperatures. In this regime N_2 is formed at higher temperatures greater than 400 ^{0}C (Fig. 3 (c)), whereas N_2O is high over a small range of temperatures (300-450 ^{0}C). The selectivity to N_2 increases as the temperature increases, up to 500 ^{0}C or so. Due to coking, at these operating conditions, very high temperatures can lead to a compromise on N_2 selectivity, in addition to reactant conversions.

At 0.6% O_2, all the reactants O_2, NO and HC conversions are 100% at higher temperatures greater than 440 ^{0}C (Fig. 4 (a)), O_2 % of 0.6% is in the optimum region where maximum NO and HC conversions are obtained. In this regime, the surface is mainly covered by CO(S) species which provide a reductive environment at lower and medium range of temperatures and at high temperature the catalyst is almost vacant (Fig. 4 (d)), indicating a very effective use of the surface area.

The gaseous products H_2O and CO decrease at higher temperatures (Fig. 4 (c)) while CO_2 and H_2 increases at higher temperatures mainly because of availability of sufficient amount of O_2 for the HC to oxidise to CO_2. At lower temperatures the main products are H_2O and CO. There is a change in product compositions and at higher temperatures the products are H_2 and CO_2.

In the optimum operating regime N_2 is formed at higher temperatures (>450) ^{0}C (Fig. 4 (c)), whereas N_2O is high over a small range of temperatures (350-450 ^{0}C). The selectivity for N_2 increases as the temperature increases. In this regime, higher temperatures are ideal from viewpoint of all aspects, HC, NO conversions, and N2 selectivity.

At 3% O_2, NO conversions are high only at low temperatures (Fig. 1 (d)) while HC conversions are maximum at low and high temperatures. O_2 concentration in the feed is in excess (Fig. 5 (a)) so this region is in the oxygen poisoned regime. After 240 ^{0}C, the catalyst is completely covered by O(S) species (Fig. 5 (d)) and provides an oxidative environment. The main gaseous products formed are H_2O and CO_2, the CO formation is very less (Fig. 5 (b)). N_2O is the major product at low temperatures, where NO conversion is reasonable (Fig. 5 (c)), whereas at high temperatures, no conversion of NO is observed. This regime is unsuitable for HC-SCR with Ag catalysts.

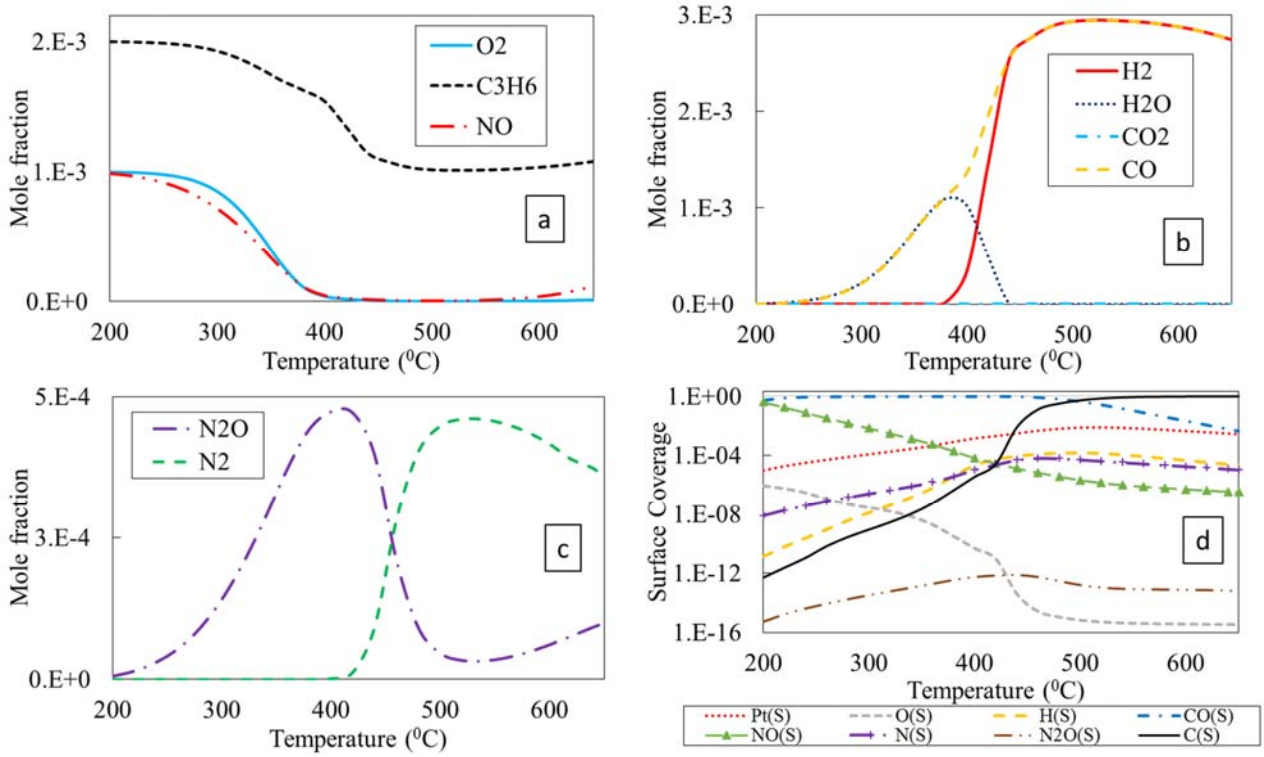

Fig. 3 (a) Mole fraction of reactants at 0.1% inlet O_2 vs reactor temperature (b) Mole fraction of H_2, H_2O, CO_2 and CO at 0.1% inlet O_2 vs reactor temperature (c) Mole fraction of N_2O and NO at 0.1% inlet O_2 vs reactor temperature (d) Surface coverage at 0.1% inlet O_2 vs reactor temperature

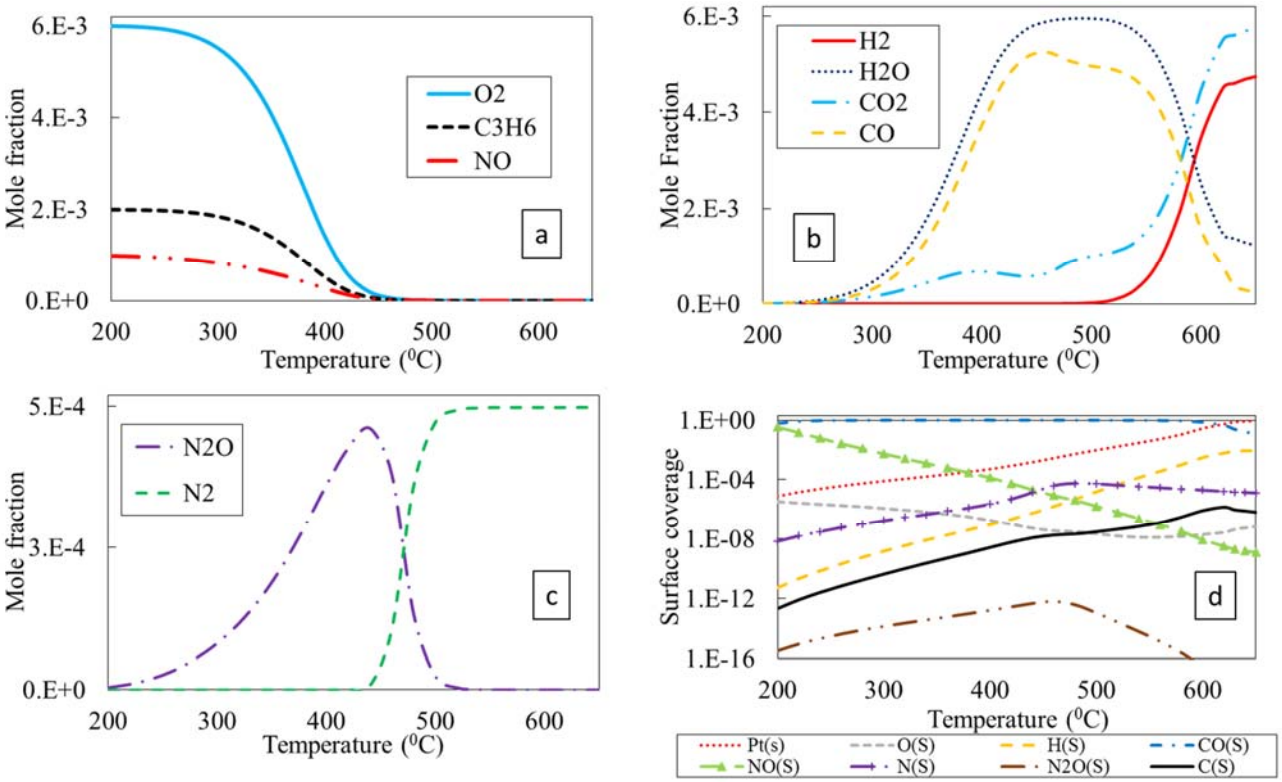

Fig. 4 (a) Mole fraction of reactants at 0.6% inlet O_2 vs reactor temperature (b) Mole fraction of H_2, H_2O, CO_2 and CO at 0.6% inlet O_2 vs reactor temperature (c) Mole fraction of N_2O and NO at 0.6% inlet O_2 vs reactor temperature (d) Surface coverage at 0.6% inlet O_2 vs reactor temperature

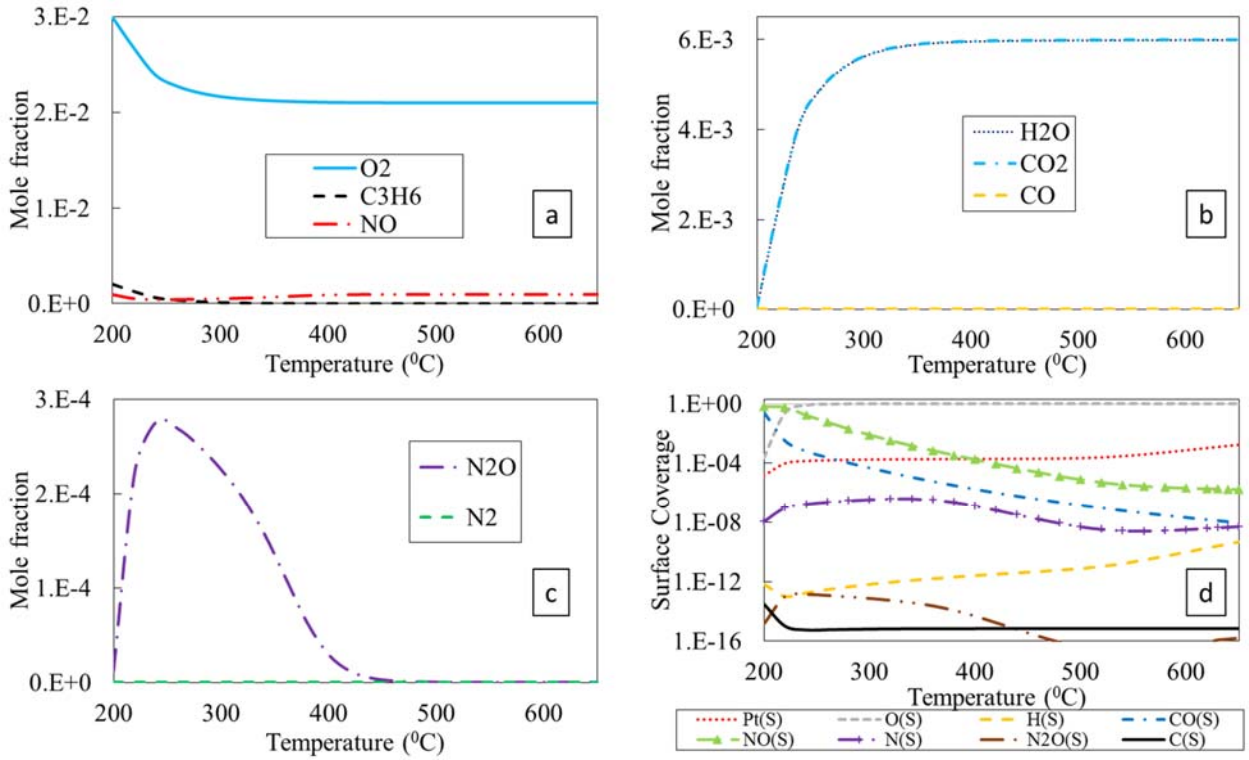

Fig. 5 (a) Mole fraction of reactants at 3% inlet O_2 vs reactor temperature (b) Mole fraction of H_2, H_2O, CO_2 and CO at 3% inlet O_2 vs reactor temperature (c) Mole fraction of N_2O and NO at 3% inlet O_2 vs reactor temperature (d) Surface coverage at 3% inlet O_2 vs reactor temperature

VI. Conclusions

The O_2 concentration is varied to determine optimal regimes of operation for HC-SCR, in an isothermal perfectly stirred reactor. At low oxygen concentrations N_2O is formed at low temperatures, and the conditions are unsuitable for HC-SCR despite high NO conversions. An optimal operating regime for maximum selectivity of NO to N_2 is found, where the conversion of NO and HC are also simultaneously high.

References

[1] Burch, R.; Millington, P.J. Selective reduction of nitrogen oxides by hydrocarbons under lean-burn conditions using supported platinum group metal catalysts. Catal. Today 1995, 26,185–206.

[2] Nikolopoulos, A.A.; Stergioula, E.S.; Efthimiadis, E.A.; Vasalos, I.A. Selective catalytic reduction of NO by propene in excess oxygen on Pt- and Rh-supported alumina catalysts. Catal. Today 1999, 54,439–450.

[3] Lee, J.H. and Kung, H.H., 1998. Effect of Pt dispersion on the reduction of NO by propene over alumina-supported Pt catalysts under lean-burn conditions. Catalysis Letters, 51(1-2), pp.1-4.

[4] Meunier, F.C.; Breen, J.P.; Zuzaniuk, V; Olsson, M; Ross, J.R.H. Mechanistic Aspects of the Selective Reduction of NO by Propene over Alumina and Silver – Alumina Catalysts. J. Catal. 1999, 187, 493–505.

[5] Luo, Y; Hao, J; Hou, Z; Fu, L; Li, R; Ning, P; Zeng, X. Influence of preparation methods on selective catalytic reduction of nitric oxides by propene over silver-alumina catalyst. Catal. Today. 2004, 93-95,797–803.

[6] Prasad, V. S; Snigdha, R; Aghalayam, P. NO reduction using Pt and Ag catalysts. Chemcon, IIT Guwahati, Dec 27-30, 2015.

[7] Chatterjee, D; Deutschmann, O; Warnatz, J. Detailed surface reaction mechanism in a three-way catalyst. R. Soc. Chem. 2001, 119,371–384.

[8] Ravikeerthi, T; Thyagarajan, R; Kaisare, N. S; Aghalayam, P. Microkinetic model for NO–CO reaction: Model reduction. Int. J. Chem. Kinet. 2012, 44,577–585.

[9] Prasad, V. S; Aghalayam, P.Microkinetic Modeling of the Effects of Oxygen on the Catalytic Reduction of NO on Pt and Rh in Automotive After treatment. IECR. 2016, 55 (35), pp 9362–9371.